catalysts

MDPI

Article

Active and Stable Methane Oxidation Nano-Catalyst with Highly-Ionized Palladium Species Prepared by Solution Combustion Synthesis

Mahmoud M. Khader *, Mohammed J. Al-Marri, Sardar Ali and Ahmed G. Abdelmoneim

Gas Processing Centre, College of Engineering, Qatar University, Doha 2713, Qatar; m.almarri@qu.edu.qa (M.J.A.-M.); ali.sardar@qu.edu.qa (S.A.); a.mohamad@qu.edu.qa (A.G.A.)

* Correspondence: mmkhader@qu.edu.qa; Tel.: +974-4403-4660

Received: 11 December 2017; Accepted: 29 January 2018; Published: 7 February 2018

Abstract: We report on the synthesis and testing of active and stable nano-catalysts for methane oxidation. The nano-catalyst was palladium/ceria supported on alumina prepared via a one-step solution-combustion synthesis (SCS) method. As confirmed by X-ray photoelectron spectroscopy (XPS) and high-resolution transmission electron microscopy (HTEM), SCS preparative methodology resulted in segregating both Pd and Ce on the surface of the Al_2O_3 support. Furthermore, HTEM showed that bigger Pd particles (5 nm and more) were surrounded by CeO_2, resembling a core shell structure, while smaller Pd particles (1 nm and less) were not associated with CeO_2. The intimate Pd-CeO_2 attachment resulted in insertion of Pd ions into the ceria lattice, and associated with the reduction of Ce^{4+} into Ce^{3+} ions; consequently, the formation of oxygen vacancies. XPS showed also that Pd had three oxidation states corresponding to Pd^0, Pd^{2+} due to PdO, and highly ionized Pd ions ($Pd^{(2+x)+}$) which might originate from the insertion of Pd ions into the ceria lattice. The formation of intrinsic Ce^{3+} ions, highly ionized (Pd^{2+} species inserted into the lattice of CeO_2) Pd ions ($Pd^{(2+x)+}$) and oxygen vacancies is suggested to play a major role in the unique catalytic activity. The results indicated that the Pd-SCS nano-catalysts were exceptionally more active and stable than conventional catalysts. Under similar reaction conditions, the methane combustion rate over the SCS catalyst was ~18 times greater than that of conventional catalysts. Full methane conversions over the SCS catalysts occurred at around 400 °C but were not shown at all with conventional catalysts. In addition, contrary to the conventional catalysts, the SCS catalysts exhibited superior activity with no sign of deactivation in the temperature range between ~400 and 800 °C.

Keywords: methane oxidation; palladium oxide/ceria catalyst; palladium oxide/ceria solid solution; solution combustion synthesis

1. Introduction

Methane (CH_4), the main constituent of natural gas plays an increasingly important role in meeting future global energy demands [1]. It is widely used in various applications such as electrical power generation and other heating applications. Unfortunately, the release of unburnt methane into the atmosphere, particularly from vehicles which are fueled with natural gas, is a serious environmental issue since it is a strong greenhouse gas with an environmental negative effect twenty times higher than that of carbon dioxide [2,3]. The conventional thermal combustion of methane not only requires very high temperatures (up to 1600 °C) but also results in production of NO_x as by-products. Thus the development of effective methane combustion catalysts would have a significant impact on a number of energy-based technologies [4,5]. CH_4 combustion promoted by heterogeneous catalysts would not only utilize the energy of methane at lower operating temperature but would also increase system performance and limit NO_x emissions by drastically reducing the required temperatures [6,7].

Catalysts based on various noble metals such as platinum (Pt), palladium (Pd), rhodium (Rh), and iridium (Ir) have been reported to exhibit considerable activities in this reaction [4,8,9]. Amongst them, palladium (Pd) based catalysts have been reported to exhibit the highest catalytic activities [10–13]. The mechanism of methane oxidation over Pd-based catalysts is complex; it relates to various factors such as the nature and redox properties of the support, oxidation state of the element active phase, particle size, and dispersion of the metal. Generally PdO_x is considered as the catalytic active phase [9,14]. However, the active phase of the catalyst is still disputed. For example, the rates of methane oxidation on PdO have been found to be larger than that on Pd^0 phase at high temperature [4,14]. However, at higher operating temperatures decomposition of PdO_x to Pd^0 was believed to be a deactivations mechanism [15–18]. It has been suggested that the most active forms of Pd-based catalysts must have a mixture of metallic Pd^0 and PdO_x [11]. The presence of atomic oxygen on the catalyst surface was proposed to be necessary for the stabilization of the intermediate CH_3 groups [17]. It has been concluded that the catalytic activities of Pd-based catalysts in CH_4 oxidation depend on the redox properties of the support and the nature of interaction of Pd with the support [10]. For low-temperature applications, Pd-based catalysts supported on alumina or zirconia have been recognized as possessing high catalytic activities [18]. However at operating temperatures above 600 °C the catalyst is deactivated through sintering and phase transformation to metallic Pd^0 [11]. Indeed, a strong deactivation dip around 550–600 °C has always been noticed with traditional Pd/Al_2O_3 impregnated catalysts of the light-off methane oxidation reaction [19,20]. Several experimental and theoretical investigations reveal that ceria stabilizes PdO_x and thus improves the catalytic activity [21–24], but pure CeO_2 has limited catalytic activity and thermal stability.

Recently uniquely structured, Pd-based core-shell catalysts have been reported [25–27], and their activities found to be higher than that of the previously best reported classical catalysts [25,26,28]. The development of the core-shell catalysts may satisfy the twin goals of high activity at lower temperatures and stability at higher temperatures. However, core-shell catalysts nonetheless appear to deactivate in the presence of steam [28,29]. It has been reported that steam deactivation is due to oxide surface hydroxylation, which might slow down oxygen mobility, and therefore reduce the methane decomposition catalytic activity [28,29]. More recently, the effect of modifying Pd/Al_2O_3 catalysts by atomic layer deposition (ALD) of ZrO_2 films was studied with the objective of forming a Pd/ZrO_2 core shell to stabilize the Pd/Al_2O_3 catalysts [30].

Recently, solution combustion synthesis (SCS) has been used to manufacture materials with relatively high catalytic activities [31–33]. In particular, palladium/ceria catalysts for oxidation reactions have evolved [23,34–38]. The oxidation catalytic activity of the palladium/ceria catalysts has been attributed to the formation of oxygen vacancies [35,36,38]. It has been debated as to whether catalytic activity is due to insertion of Pd ions into the ceria lattice or strong interaction between Pd ions and ceria [23,36,38,39].

The present study aimed to synthesize an economic methane oxidation catalyst that is active at low temperature and stable at high temperature under dry and wet conditions. An understanding of the methane oxidation mechanism is attempted. We also aimed to identify the catalyst active phase through correlation of the activity to surface composition. In addition, the study aimed to quantify catalytic activity of the solution-combustion synthesis (SCS) catalyst and benchmark to that of a traditional catalyst.

2. Results and Discussion

2.1. Catalyst Characterization

2.1.1. Catalyst Surface Morphology

To afford detailed insights into the structural properties of the catalyst nanoparticles (NPs), high-resolution transmission electron microscopy (HTEM), Figure 1. Fast Fourier transformation (FFT) and energy dispersive X-ray (EDX) analysis were conducted on the 5P5CA sample, Figure 2. Direct

evaluation of the HTEM and the High-Angle Annular Dark-Field (HAADF) images showed that crystalline nanoparticle (NPs) of Pd/CeO_2, in the range 1–50 nm, were observed on the Al_2O_3 support, Figure 1b. It was obvious from the HAADF image that heavier metals (Pd and Ce) were segregated on the Al_2O_3 surface, Figure 1b; confirming the upcoming X-ray photoelectron spectroscopy (XPS) results (Table 1). The analysis of the bigger NPs (5 nm and above) by the FFT, inverse FFT and EDX mapping, Figure 2a–c, respectively, showed that these NPs were double-domain aggregates of Pd and CeO_2 structures. In these double domains, the Pd NPs were surrounded by CeO_2 NPs, as clearly shown in Figure 2d; resembling a core-shell nanostructure. As can be seen in Figure 3, the small particles (~<1 nm in size) were also detected by HAADF but with insufficient contrast against background noise originating from the support, which showed mono-domain with d-spacing = 2.2 Å which is a typical characteristic of Pd NPs [40]. In the case of the 5P5C-SCS nanocatalyst, the formation of core-shell nanostructures is suggested to play a major role in catalytic activity and stability during the methane oxidation reaction. As proved in the reported literature, core-shell nanostructures resulted in enhanced interactions by maximizing the interfaces between Pd and CeO_2. The catalytic activities of Pd-based core-shell catalysts for application to methane oxidation were reported to be exceptionally higher than that of the previously best reported catalysts [25,26,28]. The exceptionally high catalytical performances of the core-shell catalysts were attributed to the efficient oxygen back-spillover, resulting from the expected core-shell structure. Even though, the SCS methodology has been used to manufacture materials with high catalytic activities [31–33] the high catalytic activity of the Pd-based SCS catalysts has been attributed to the formation of oxygen vacancies as well as to the formation of metal-substrate solid solution. However, the formation of the core-shell arrangement via SCS synthesis has not been reported. These differences could be attributed to a difference in the synthesis conditions as well as a difference in the catalyst composition.

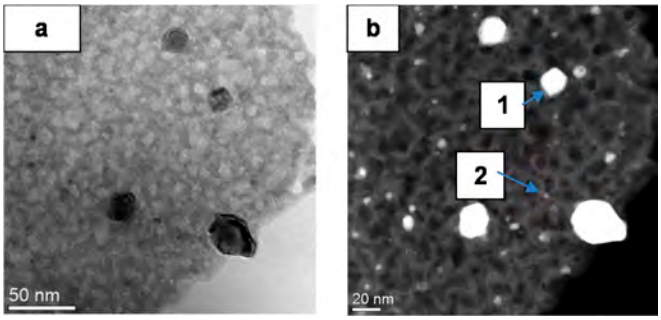

Figure 1. Images of (**a**) the transmission electron microscope (TEM) and (**b**) the High-Angle Annular Dark-Field (HAADF) for 5P5C-SCS catalyst. SCS = solution-combustion synthesis.

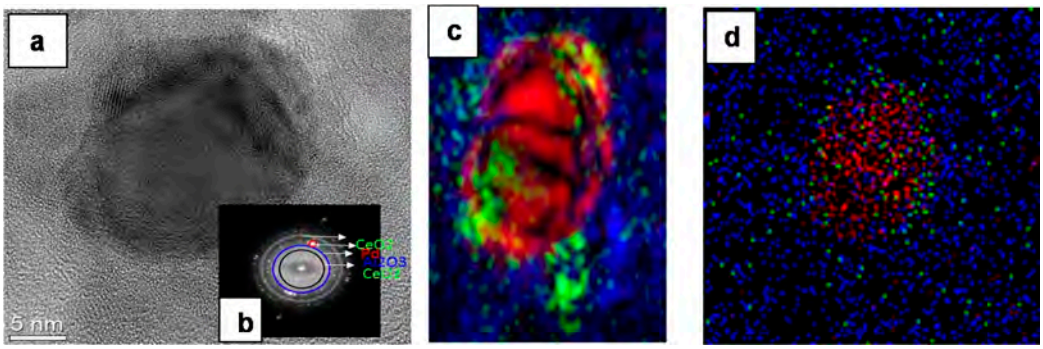

Figure 2. (**a**) High resolution TEM (HRTEM) image of particle 1 from Figure 1b; (**b**) its fast Fourier transformation (FFT) mode, (**c**) Inverse FFT (pseudo-DF), and (**d**) EDX map. The colors in Figure 2c,d: blue = Al, green = Ce and red = Pd.

Table 1. Quantitative analysis of surface composition obtained from X-ray photoelectron spectroscopy (XPS) analysis [a].

	$Ce(3d_{5/2})$		$Pd(3d_{5/2})$			$Al(2p_{3/2})$	O1s
1P5C-SCS	9.84 ± 0.64			1.29 ± 0.27			
	Ce(III)	**Ce(IV)**	**Pd^0**	**Pd^{2+}(PdO)**	**$Pd^{(2+x)+}$** [b]	44.75 ± 0.4	43.81 ± 0.5
	43.44 ± 2.8	56.56 ± 2.8	29.17 ± 3.2	36.84 ± 2.6	32.98 ± 5.4		
2.5P5C-SCS	**$Ce(3d_{5/2})$**			**$Pd(3d_{5/2})$**			
	12.82 ± 0.82			2.28 ± 0.14		43.236 ± 0.4	41.65 ± 0.4
	Ce(III)	**Ce(IV)**	**Pd^0**	**Pd^{2+}(PdO)**	**$Pd^{(2+x)+}$** [b]		
	49.92 ± 4.6	50.07 ± 4.6	30.36 ± 2.7	46.16 ± 4.7	24.29 ± 1.7		
5P5C-SCS	**$Ce(3d_{5/2})$**			**$Pd(3d_{5/2})$**			
	8.82 ± 0.26			2.95 ± 0.25		45.10 ± 0.3	42.92 ± 0.5
	Ce(III)	**Ce(IV)**	**Pd^0**	**Pd^{2+}(PdO)**	**$Pd^{(2+x)+}$** [b]		
	41.17 ± 1.8	58.42 ± 1.8	32.63 ± 5.5	41.95 ± 3.2	25.71 ± 2.3		
5P5C-I	**$Ce(3d_{5/2})$**			**$Pd(3d_{5/2})$**			
	3.63 ± 1.3			4.52 ± 0.23		47.23 ± 0.4	44.62 ± 0.4
	Ce(III)	**Ce(IV)**	**Pd^0**	**Pd^{2+}**	**$Pd^{(2+x)+}$** [b]		
	0	100	13.2	86.8	0		

[a] Above table represents average values calculated from five etching cycles. [b] Highly ionized Pd (Pd^{2+} species inserted into the lattice of CeO_2). SCS = solution-combustion synthesis

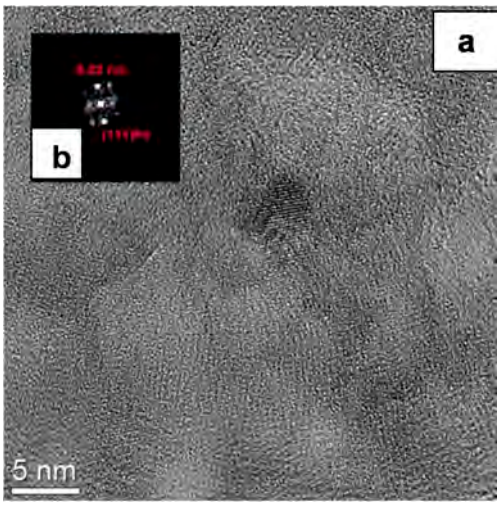

Figure 3. (**a**) HRTEM and (**b**) FFT images of small particle (2) from Figure 1b.

2.1.2. X-ray Diffraction Analysis

XRD patterns of the calcined samples are displayed in Figure 4. As can be seen, for pure CeO_2 the *hkl* reflections at (111), (200), (220), (311), (222), (400), and (331) at 2θ values of 28.54, 33.02, 47.32, 56.42, 58.46, 69.98, 76.04, and 78.28 were attributed to the characteristic diffraction patterns of cubic ceria (CeO_2) [41]. The XRD pattern of the 5P5C-I catalyst revealed the presence of the metallic Pd^0 phase at 2θ value of 38.86 (see Figure 4c). However, the diffraction lines corresponding to PdO were not observed. The diffraction lines of various phases of Al_2O_3 were also recorded at 2θ values of 45.2 and 66.4 [42]. The diffraction lines at 2θ values of 28.6 and 47.5 indicated the presence of cubic CeO_2 [43]. By contrast, the XRD patterns of the 5P5C-SCS nanocatalyst revealed the presence of PdO as well as metallic Pd^0. As shown in Figure 4b, PdO phases were evidenced from the (111) and (103) peaks at 2θ values of 41.32 and 60.22, respectively. Metallic Pd^0 was evidenced from the (111) peak at 2θ value of 38.86. Moreover the characteristic diffraction lines for Al_2O_3 (at 2θ values of 37.1, 45.2, and 66.4) were also recorded. As shown, the characteristic diffraction peaks corresponding to Pd^0 and PdO phases were broad and comparatively weak indicating smaller and/or well dispersed Pd species over the substrate. It was worth noticing that the XRD analysis in the case of the 5P5C-SCS

nanocatalyst strongly suggested the following main points; (a) The experimental lattice constant of CeO_2 in 5P5C-SCS nanocatalyst (5.416 ± 0.0018 Å) was larger than that of the pure CeO_2 sample (5.411 ± 0.0018 Å) and (b) broadening of the diffraction lines of CeO_2. This strongly indicated the substitution of Pd^{2+} ions with Ce^{4+} ions in the crystal lattice of CeO_2 and resulted in the formation of PdO/CeO_2 solid solution. Indeed, it has been suggested that since Pd^{2+} and Ce^{4+} ions have very similar ionic radii and as a result of the molecular level homogenosity (as in the present) in solution of the precursor salts of these ions, the palladium cations could easily be induced into the ceria lattice structure [37]. It could be concluded from the XRD analysis results that SCS synthesis methodology resulted in the formation of three main types of the catalyst nanocrystallite components i.e., metallic Pd^0, PdO_x, and PdO/CeO_2 solid solution. Indeed, the findings from XRD analysis were in good agreement with the results of XPS analysis.

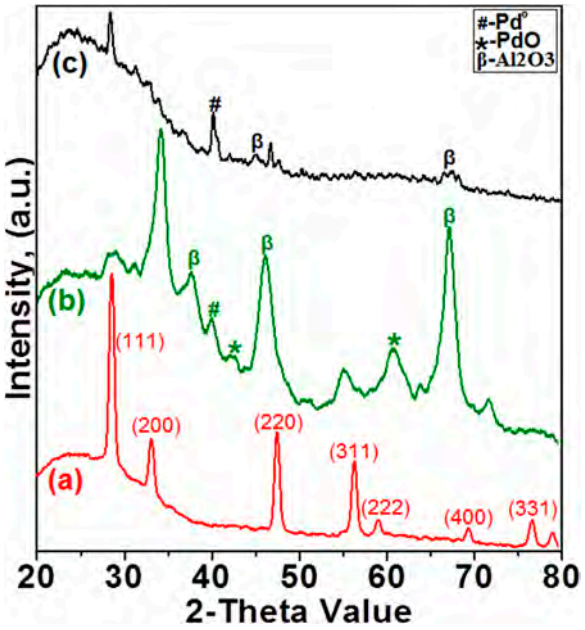

Figure 4. X-ray diffraction (XRD) patterns of the calcined samples (**a**) calcined pure CeO_2 prepared via the SCS method; (**b**) 5P5C-I; (**c**) 5P5C-SCS.

2.1.3. X-ray Photoelectron Spectroscopy (XPS) Studies

The surface chemical composition and distribution of Pd species at the surface of the calcined catalysts were investigated by XPS. As demonstrated in Figure 5a, the Pd3d spectrum of 5Pd-I catalyst with the binding energies of 335.97 eV and 341.52 eV indicated that Pd was predominately present in the chemical state of PdO. The Pd3d spectrum (Figure 5b) of 5P5C-I catalyst exhibited the presence of Pd^{2+} and metallic Pd^0. This the XPS spectrum was characterized by two doublet Pd3d peaks: the binding energies 336.41 eV and 341.82 eV were assigned to PdO, whereas the second doublet at binding energies at 334.91 eV and 339.92 eV was assigned to Pd^0 [44–46]. In the XPS spectra of the Ce(3d) core level region of the 5P5C-I (Figure 5c) the $Ce3d_{3/2}$ and $3d_{5/2}$ appeared at 919.29 eV and 884.39 eV respectively with well separated spin-orbit components (Δ = 16.1 eV) having multiple splitting-typical of Ce^{4+} in CeO_2 [23]. Contrary to both impregnation catalysts, the XPS spectra of the 5P5C-SCS sample showed much broader and less symmetrical peaks indicating a larger heterogeneity in its palladium environments. The XPS of the Pd(3d) core level region of the 5P5C-SCS (Figure 5d) showed three $Pd(3d_{5/2,3/2})$ peak doublets. The binding energies at 335.12 and 336.32 eV were assigned to $Pd(3d_{5/2})$ in Pd metal and PdO, respectively [44,46–51]. The third doublet with its $Pd(3d_{5/2})$ peak at 337.82 eV was assigned to Pd ions but was more ionized than those associated with PdO. A similar peak was assigned by Venezia et al. and Bi et al. to Pd^{4+}, as in PdO_2, due to the oxygen incorporation into

the PdO crystal lattice during calcinations [52]. The highly ionized Pd ions of the samples prepared by the SCS can also be assigned to Pd ions which were inserted into the ceria lattice forming pallida/ceria solid solution [23,38,53]. The appearance of the three Pd XPS doublets, comparing to only two Pd XPS doublets for the impregnation catalyst, strongly indicated the formation of Pd/ceria solid solution as has already been reported in recent literature [23,36,38]. In the theoretical study by Scanlon et al. [54], it was predicted that the ground state structure of Pd doped CeO_2 is a square planar with Pd ions having d^8 configuration; meaning that Pd^{2+} rather than Pd^{4+} is the predominant oxidation state in the Pd-O-Ce solid solution linkage. These Pd^{2+} ions should have a greater ionic property than the Pd^{2+} ions of normal PdO. Therefore, it is plausible to assign the high-energy Pd XPS doublet at 337.82 eV to the strongly ionized Pd^{2+} ions inserted into the Pd-O-Ce solid solution linkage.

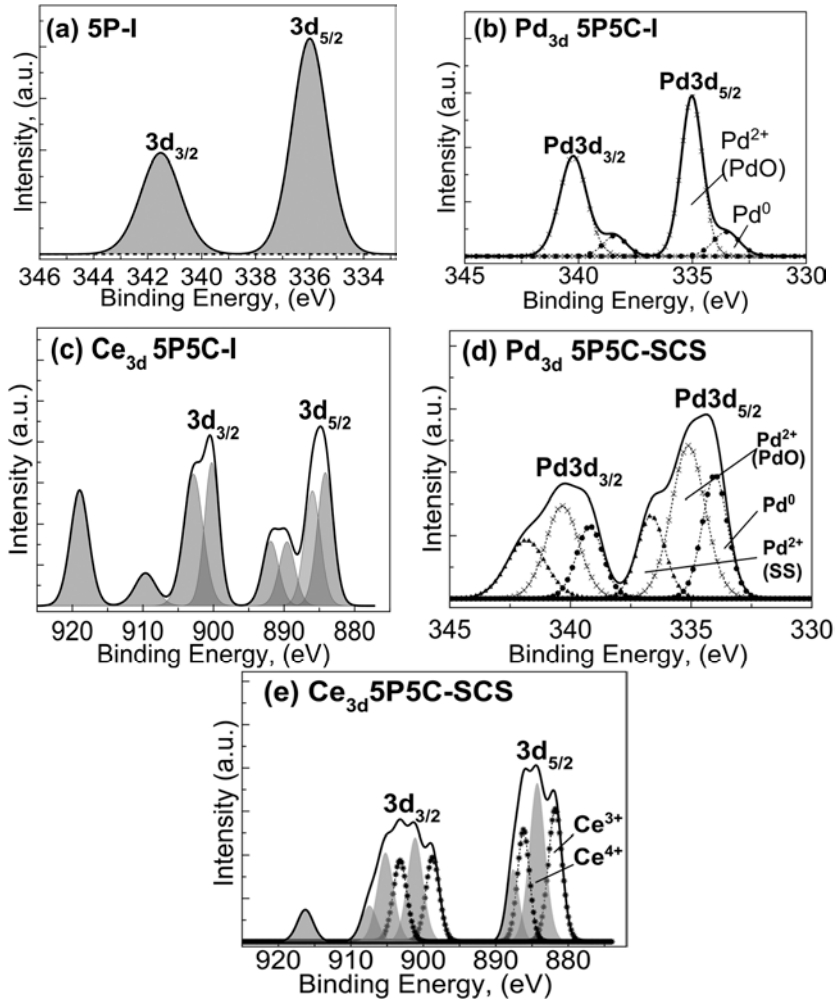

Figure 5. Representative XPS Pd3d and Ce3d core-level spectra of the catalysts (**a**) Pd3d in 5P-I; (**b**) Pd3d in 5P5C-I; (**c**) Ce3d in 5P5C-I; (**d**) Pd3d in 5P5C-SCS; (**e**) Ce3d in 5P5C-SCS.

Table 1 represents the XPS surface elemental analysis of the three catalysts. The data in this table strongly suggested the following main points: (a) ceric ions segregated to the surface as the ceric composition was ~10% (originally, 5% was used in preparing the three catalysts); (b) The surface segregation of Pd on the surface of the 1P5C-SCS catalyst indicated that most of the Pd was diffused to the surface. Conversely, the 5P5C-SCS catalyst indicated a lower surface Pd content than expected, presumably due to Pd diffusion into the bulk of the material. Indeed, the XRD clearly showed metallic as well as PdO in the bulk of this catalyst, indicating that not all the Pd was inserted into the ceria lattice. (c) There was a proportional increase in the highly ionized Pd^{2+} ions on increasing the Pd loading in

the original preparations, as clearly shown in their linear relationship (Figure 6). This straight-line relation predicted that there were non-stoichiometric compounds formed between Pd and CeO_2 associated with the formation of the oxygen vacancy, $\ddot{V}_{O^{2-}}$, to maintain the charge neutrality in the overall palladium/ceria lattice. Based on these results, it is reasonable to suggest that, in contrast to the conventional method, Pd was inserted into the ceria lattice during the SCS forming a non-stoichiometric Pd-O-Ce solid solution, which was segregated on the surface of the alumina support. This explanation corroborates the conclusions of the experimental work by Colussi et al. [23,38] and Priolkar et al. [36] as well as the theoretical prediction by Scanlon et al. [54]. The insertion of Pd ion into the ceria lattice must be associated with oxygen vacancy formation and, consequently, with the generation of Ce^{3+} ions. Indeed, XPS (Figure 5e) showed the formation of Ce^{3+} ions in all catalysts prepared by the SCS, though these catalysts were formed under oxidation conditions during the SCS. It was evident that the XPS of the catalyst 5P5C-I, prepared by impregnation, revealed no Ce^{3+} peaks (Figure 5c).

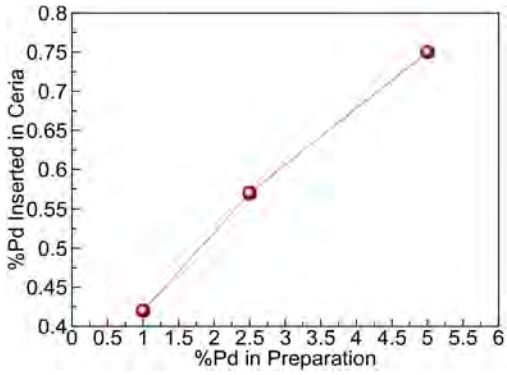

Figure 6. The relationship between the % of Pd added to the solution in the SCS and the % of Pd inserted in the ceria lattice. Inserted Pd concentration was measured by XPS for the peak for the highly ionized Pd positioned at 337.82 eV.

The suggested schematic below showing the oxygen ion vacancy, associated with a strongly ionized Pd^{2+} and Ce^{3+} ion in the SCS catalysts is shown in Figure 7.

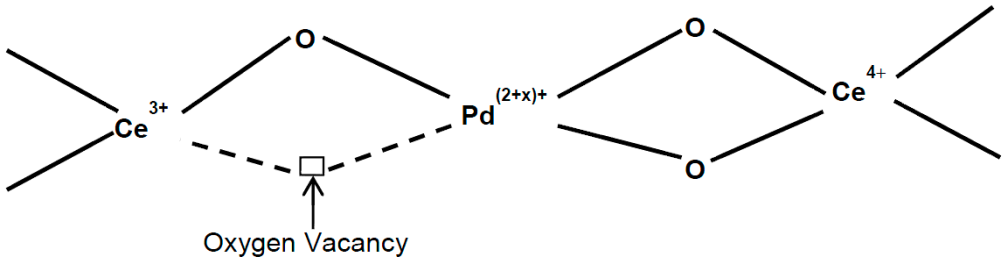

Figure 7. Schematic representation of the suggested palladium oxide/ceria solid state solution formed during the SCS.

2.1.4. Sequential Temperature Programmed Reduction (TPR) and Temperature Programmed Oxidation (TPO)

For ceria to act effectively as an oxygen storage component, the reduction and/or oxidation processes must be readily reversible. Sequential temperature programmed reduction/oxidation was therefore employed to establish the ease with which reduction and re-oxidation of the catalyst occurs. The temperature programmed reduction (TPR) profile of the 5P5C-SCS nanocatalyst in hydrogen is shown in Figure 8a. As can be seen, there were several low temperature peaks (below 150 °C), one middle reduction peak (288 °C), and two high temperature peaks (higher than 600). Reduction peaks at 69 °C, 92 °C and 116.6 °C were attributed to the surface oxygen species from PdO reduction.

The two high-temperature peaks at 615 °C and 835 °C respectively, were ascribed to surface and bulk reduction of ceria [55,56]. The middle temperature peak at 288 °C could be assigned to the reduction oxygen adsorbed on the intrinsic point defects created due to the Pd insertion in the ceria lattice. A similar low oxygen reduction peak was observed by Zhang et al. [55] and was attributed to molecular oxygen adsorbed on vacancies which were generated on the ceria nanowires synthesized by these authors. Another explanation of the low temperature H_2-TPR peak could be due to the formation of superoxo-species (O_2^-) formed from charge transfer on the surface and near-surface Ce^{3+} ions [57]. After recording the H_2-TPR the reduced sample was submitted to an oxygen-containing atmosphere and was then heated to 900 °C. As can be seen in Figure 8b, a series of O_2 consumption peaks in the temperature range between 50 °C and 850 °C were recorded. These peaks were attributed to reoxidation of various reduced species of palladium and partially reduced CeO_2. Indeed the results of sequential H_2-TPR/TPO analysis gave a strong indication that reduction as well as consequent reoxidation of the 5P5C-SCS nanocatalyst occurred readily.

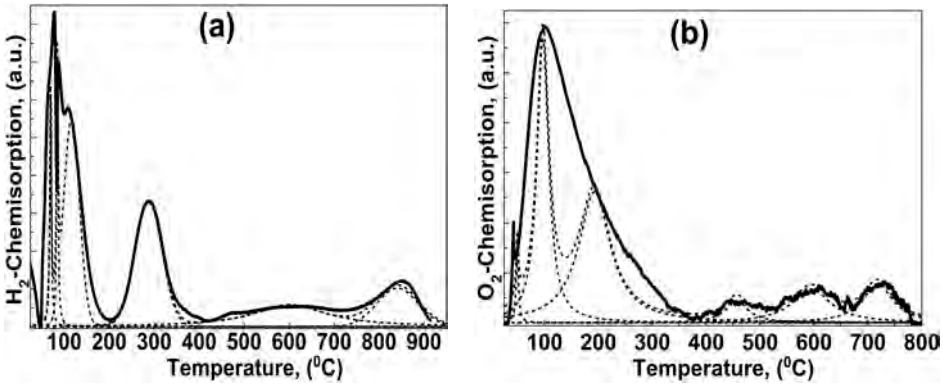

Figure 8. Sequential TPR/TPO profiles of the 5P5C-SCS nanocatalyst. (**a**) Hydrogen temperature programmed reduction (H_2-TPR) and (**b**) temperature programmed oxidation (TPO).

2.2. Catalytic Activity

For all samples, the reaction rates of methane oxidation were measured at a temperature of 550 °C. The rates of methane decomposition over 5P5C-SCS, 5P-I and 5P5C-I catalysts were recorded to be 1077.55 μmol (g Pd)$^{-1}$ s^{-1}, 57.06 μmol (g Pd)$^{-1}$ s^{-1}, and 60.82 μmol (g Pd)$^{-1}$ s^{-1}, respectively. The results revealed that samples prepared by SCS were exceptionally more active than the catalysts prepared by the conventional impregnation method. As can be seen in Table 2, the reaction rate over 5P5C-SCS catalyst was higher by a factor of ~18 times than that of 5PdI and 5PdC-I catalysts. The difference in the catalytic performances amongst the catalysts was attributed to the difference in surface chemical species of palladium present on the surface as previously discussed.

Table 2. Physicochemical properties and methane combustion rates of the samples.

Sample	Pd (wt%) [a]	S.A. (m^2 g^{-1}) [b]	Rate of Methane Decomposition [c] (μmol (g Pd)$^{-1}$ s^{-1})
5P-I	4.84	-	57.06
5P5C-I	4.52	54.28	60.82
5P5C-SCS	2.95	100.56	1077.55

[a] Measured by XPS analysis. [b] BET surface area. [c] Reaction rates measured at 550 °C.

The qualitative conversion profiles demonstrated the effects of preparative methodology and chemical structure on the catalytic activities and stabilities as a function of reaction temperature. As can be seen in Figure 9a, in the case of the 5Pd-I sample after the light-off at 250 °C, the catalytic activity started increasing and finally reached a maximum of 85% of conversion of methane at ~500 °C.

However, with further heating a strong deactivation dip for CH_4 oxidation in the range of 500–750 °C was observed. It was worth noticing that with the 5Pd-I catalyst a complete conversion of methane was never achieved. Generally, PdO_x has been recognized as the catalytic active phase. This drop in the conversion of methane with the reaction temperature has been reported in numerous studies and was attributed to the decomposition of catalytically active PdO_x to comparatively less active Pd^0 species [18,19]. This resulted in a decrease in the rate of methane combustion and hence a transient dip in the activity was observed. The same interpretation might hold for the 5Pd-I catalysts. Moreover, the transient deactivation was more evident during the cooling cycle. This was because with decrease in reaction temperature, the re-oxidation of Pd^0 to the more active PdO was reported to be kinetically less favorable [34].

In order to overcome the drawback associated with the conventional Pd/Al_2O_3 catalysts, both theoretical and experimental investigations have suggested that the incorporation of ceria into Pd-based methane oxidation catalysts can result in improved catalytic activity and stability [21,58–60]. For example Sheedeh and co-workers reported a comparative investigation of the activity of various Pd-based catalysts for application to methane oxidation. These catalysts were dispersed over various oxide supports such as Al_2O_3, CeO_2, and Al_2O_3 doped with 20 wt% CeO_2. They concluded that the catalyst with $Pd/CeO_2Al_2O_3$ formulation resulted in a significant improvement of the activity during methane combustion [58]. However, the activity of ceria promoted Pd-based was highly dependent on preparative methodology and the nature of interaction of Pd with ceria. For example, a weaker interaction between PdO_x and CeO_2 may lead either to surface segregation of Pd or migration of Pd to bulk of the material [36,37,61]. As can be seen in Figure 9b, the impregnation of 5 wt% CeO_2 into the 5Pd-I catalyst had a dramatic effect on the light-off curves. First, light-off temperatures for methane oxidation shifted to higher values by approximately 200 °C for both the heating and cooling cycles. Second, transient deactivations did not appear during both the heating and cooling cycles. This suggested that the addition of CeO_2 to PdO_x resulted in comparatively less activity at low reaction temperature but increased stability at high reaction temperature. The lower activity of this catalyst could possibly be due to either of the aforementioned factors. As mentioned in the earlier section the XPS analysis of 5P5C-I catalyst showed Pd was mainly present in the chemical state of PdO. This indicated that Pd did not insert into the ceria lattice and hence a low activity was recorded during methane oxidation. This observation was also in accordance with earlier reports that incorporation of ceria may result in stabilization of PdO, only if good interaction between the CeO_2 and the Pd was achieved [62–64].

The reported results of qualitative conversion profiles over the Pd-based catalysts developed via SCS technique provided evidence that the 5P5C-SCS nano-catalyst was superior in activity and stability than that of the conventional 5P-I and 5P5C-I catalysts. Firstly, the novel 5P5C-SCS catalyst demonstrated exceptionally high activity for methane oxidation below 400 °C. As shown in Figure 9c the beginning of light-off for 5P5C-SCS was observed at 200 °C compared to the 250 °C and 520 °C temperature required for the 5P-I and 5P5C-I catalysts respectively, prepared by the conventional impregnation method. Methane conversion over 5P5C-SCS increased with increasing operating temperature with full conversion attained at around 410 °C. It was worth noticing that under similar reaction conditions, complete combustion of methane over conventional 5P-I and 5P5C-I catalysts was never achieved. Secondly, contrary to the conventional 5P-I and 5P5C-I catalysts, the 5P5C-SCS nanocatalyst exhibited superior activity with no sign of deactivation in the temperature range between ~400 and 800 °C. This behavior of the SCS catalysts resembled the core shell catalysts that have made a breakthrough in methane oxidation research [25,34]. On the other hand, the SCS catalysts were superior to the traditional catalysts which all showed significant deactivation at high temperature [15,19,20]. This exceptionally high activity at low temperature (>400 °C) and absence of a deactivation hump at high operating temperature (400–800 °C) during methane combustion over 5P5C-SCS nanocatalyst could be associated with the unique physicochemical properties of the Pd-SCS catalysts. Firstly, as confirmed by X-ray photoelectron spectroscopy (XPS) and high-resolution transmission electron

microscopy (HTEM), SCS resulted in segregating the Pd and Ce on the Al_2O_3 surface. Secondly, oxygen vacancies were formed because of the insertion of Pd ions into the ceria lattice. The findings of HTEM analysis showed that bigger Pd particles (5 nm and more) were surrounded by CeO_2, resembling a core shell structure, while smaller Pd particles (1 nm and less) were not associated with CeO_2. The intimate Pd-CeO_2 attachment due to core-shell formation might have resulted in insertion of Pd ions into the ceria lattice, associated with the reduction of Ce^{4+} into Ce^{3+} ions and so presumably the formation of oxygen vacancies. Indeed, as discussed in the earlier section, the results of XRD analysis strongly suggested also that the substitution of Pd^{2+} ions with Ce^{4+} ions in the crystal lattice of CeO_2 resulted in the formation of a solid solution and oxygen vacancies. The XPS analysis affirmed the findings of HR-TEM and XRD results. XPS showed also that Pd had three oxidation states corresponding to Pd^0, Pd^{2+} due to PdO and highly ionized Pd ions ($Pd^{(2+x)+}$) which might have originated from the insertion of Pd ions into the ceria lattice. XPS showed that also that palladium oxide/ceria enriched the surface of the alumina support; its intrinsic Ce^{3+}, oxygen vacancies and highly ionized Pd suggested playing a major role in the unique catalytic activity. Indeed, there is also reported literature to suggest that SCS synthesis methodology resulted in catalysts with comparatively higher activity than that of the catalysts prepared via conventional impregnation methods. For example S. Specchia et al. reported the synthesis of 2% Pd supported over Ceria-Zirconia via the solution combustion (SCS) method [35]. From the results of surface chemical characterization techniques of oxygen temperature programmed desorption, hydrogen temperature programmed reduction and infrared spectroscopy of low temperature carbon monoxide adsorption, they concluded that the presence of small metallic palladium (Pd^0) particles together with well dispersed PdO_x species were responsible for higher catalytic activity for methane combustion at low operating temperatures. Similarly, the lower catalytic activity was ascribed to be due to the oxidation of Pd^0 to the least active PdO_x species. S. Colussi and co-workers also reported the synthesis of Pd-based and Pt-based catalysts supported either over CeO_2 or Al_2O_3 via the SCS method [65]. These catalysts were evaluated for activity in the combustion of propane and dimethyl ether (DME). They reported that the catalysts prepared via the SCS method exhibited higher activity than the conventional impregnation catalysts. On the basis of high resolution transmission electron microscopy (HRTEM) results the enhanced catalytic activity was ascribed to the existence of PdO_x and nanosized zarovalent Pd particles. In the aforementioned reported work CeO_2 and CeO_2-ZrO_2 were used as catalytic supports which are considerably expensive materials [35,65]. By contrast, the results of XPS and HRTEM analysis of the Pd-based SCS catalysts reported in this work suggested that most of the palladium and ceria (the key catalytic components) nanocrystallites were segregated on the surface of the alumina support. Indeed, this could be an additional advantage of these catalysts as the active and stable catalyst could be developed with as low as 1 wt% PdO_x and 5 wt% of CeO_2 dispersed over alumina as carrier (see Figure 9).

Based on the catalytic activity results, it is reasonable to conclude that the presence of inserted Pd^{2+} ions in the ceria lattice, small or high concentration, and/or an intimate interaction between Pd and CeO_2, were key to achieving superior methane combustion activity and stability. The formation of oxygen vacancies was in agreement with the results of Priolkar and co-workers [36]. They reported that the 1 wt% Pd/CeO_2 catalyst synthesized via solution combustion method exhibited higher catalytic activity for CO oxidation and NO reduction than the Pd/CeO_2 catalysts prepared by the conventional impregnation method. From the results of surface chemical characterization techniques of XRD, XPS and extended X-ray absorption fine structure (EXAFS) spectroscopy, they concluded that the Pd^{2+} ions get stabilized in the Ce^{4+} sites resulting in the formation of $Ce_{1-x}Pd_xO_{2-\delta}$ type of solid solution. The high activity of this catalyst for CO oxidation and NO reduction was attributed to the formation of a Pd-O-Ce solid solution on Pd/ceria catalyst. Intrinsic Ce^{3+} ions and oxygen vacancies, associated with the insertion of Pd^{2+} ions into ceria lattice, activate oxygen adsorption as evidenced by the 288 °C H_2-TPR peak (Figure 8a). The adsorption of O_2 on oxygen vacancies, presumably followed by its dissociation is expected to play a major role in the oxidation reaction. It is generally accepted that the prevalent mechanism of the high temperature CH_4 catalytic oxidation

involves a redox Mars-van Krevelen-type reaction [20,34,66]. In the present catalysts, the point of interaction between Pd and CeO_2 and/or the intrinsic oxygen vacancies presumably acted as centers for dissociating molecular oxygen into chemisorbed oxygen (O*) which were then consumed in the oxidation reaction. The oxygen vacancy then replenished by gas-phase oxygen thereby completing the cycle by formation and desorption of CO_2 and H_2O. Indeed, a further demonstration that the PdO_x phase was comparatively more active than that of the Pd^0 phase was supported by exposing a sample of the reduced catalyst to the methane oxidation gas mixture, this sample showed an initial deterioration in its activity as is clearly shown in Figure 10. The comparatively lower activity of the reduced catalyst also further indicated that the Mars-van Krevelen mechanism was operative at high temperature. As demonstrated in Figure 10, when the reactants feed mixture was introduced to the reduced catalyst at operating temperature of 500 °C, the activity started with around 82% of methane decomposition only, rather than 100% as in the case of oxidized catalysts. However, the catalyst regained its activity instantaneously. This behavior was presumably, due to the removal of surface oxygen by hydrogen reduction such that it reduced its participation in CH_4 oxidation. Consequently, the catalytic activity also declined. However, this instantaneous regain in catalytic activity upon exposure to the reactants feed (O_2 and CH_4) might be due to surface oxidation of Pd^0 to more active PdO_x species followed by methane oxidation via PdO_x.

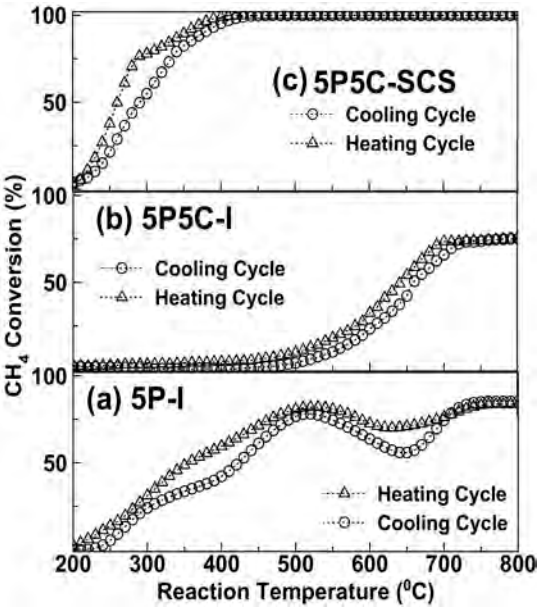

Figure 9. Catalytic performance for methane oxidation as a function of reaction temperature for (**a**) 5 wt% Pd/Al_2O_3 (5P-I) impregnation catalyst (**b**) 5 wt% Pd 5 wt% CeO_2/Al_2O_3 (5P5C-I) impregnation catalyst and (**c**) 5 wt% Pd 5 wt% CeO_2/Al_2O_3 SCS catalyst (5P5C-SCS). Light-off measurements were carried out with 30 mg of catalyst at a total gas pressure of 1 atm with CH_4 (5% CH_4/Ar) to O_2 (5% O_2/Ar) v/v ratio of 2. Catalyst was activated by treating them with 30 mL min^{-1} of 5% O_2/Ar at 550 °C at a heating rate of 10 °C min^{-1}.

Further to the evidence that the exceptionally high activity of the Pd-SCS catalyst was due to the high ionized $Pd^{+(2+)}$ species, a set of three catalysts were also synthesized via the SCS method. In these catalysts, the weight percentage of CeO_2 was fixed at 5 wt%, while the Pd loading was varied from 1 wt%, 2.5 wt%, and 5 wt%. Figure 11, demonstrates the qualitative light-off curves of the three catalysts with different Pd loadings. As can be seen, increase in Pd content appeared to induce a further increase in the catalytic performance in the low temperature region (>400 °C). Most importantly, the temperature at which 90% of CH_4 was oxidized, T_{90}, decreased from 402 °C to 378 °C and to 355 °C with increase in Pd loading from 1% to 2.5%, and 5%, respectively. This result was in accordance with

the findings of XPS analysis results. As discussed earlier, increase in Pd loading resulted in an increase in the fraction of highly ionized $Pd^{+(2+)}$ species. The 5P5C-SCS nanocatalyst was comparatively more active in the low temperature region. This was because, the highly ionized $Pd^{+(2+x)}$ species were found to be highest in concentration and were segregated on the Al_2O_3 surface.

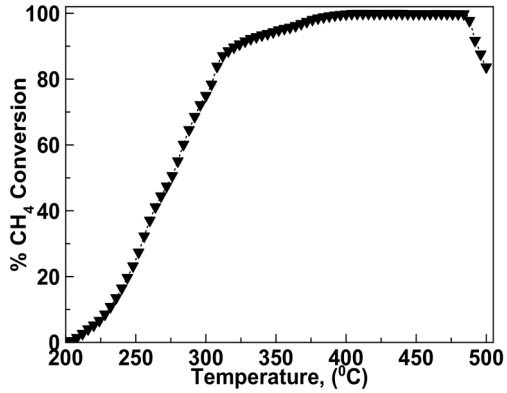

Figure 10. Effects of reductive pretreatment on the methane oxidation over 5P5C-SCS catalyst. The catalyst was first reduced at 300 °C in a stream of 30 mL min^{-1} of pure H_2, and then heated in flowing H_2 till the temperature reached 500 °C and flushed with Ar for 20 min. Ar was then replaced by mixture of 5% CH_4/Ar and 5% O_2/Ar with O_2/CH_4 v/v ratio of 2 while the temperature was continuously lowered.

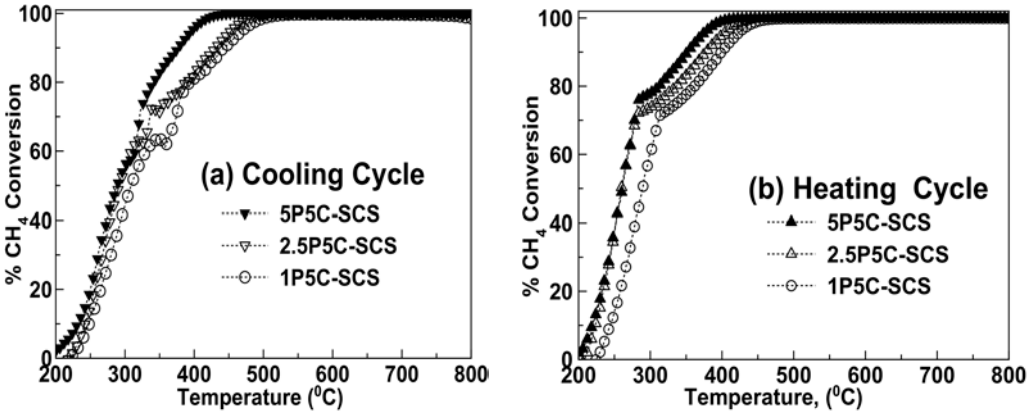

Figure 11. Catalytic performance for methane oxidation as a function of reaction temperature for catalysts made of fixed 5% CeO_2 and varied Pd composition (the balance is Al_2O_3).

One more formulation of the catalyst (denoted as 5P5C-A) was also synthesized with the objective to investigate the effects of the type of alumina support on the catalytic activity during methane oxidation. The weight percentages of Pd and CeO_2 were 5 wt% each supported over Al_2O_3. In this case, as a first step, the alumina support was prepared by the SCS method followed by the addition of Pd and CeO_2 via wet impregnation. A comparison between catalytic activity during methane oxidation over 5P5C-SCS and 5P5C-A was performed to eliminate any difference among the two catalysts caused by the type of alumina used as support. Figure 12 demonstrates a comparison of the light-off curves during methane oxidation over the 5P5C-SCS and 5P5C-A catalysts. As can be seen, the 5P5C-A catalyst exhibited a trend similar to that of the 5P5C-I impregnation catalyst. Indeed, it might be reasonable to conclude that the alumina support only served to disperse the active Pd-CeO_2 phase and did not participate in the main reaction.

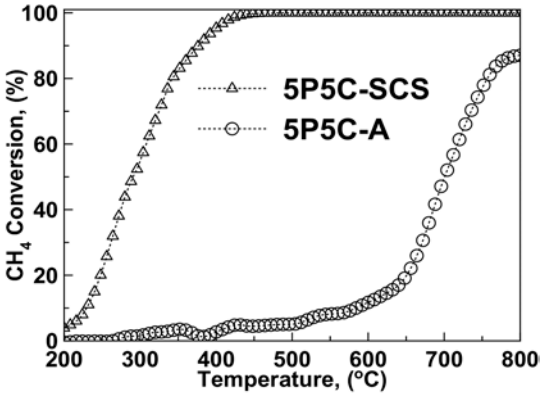

Figure 12. Catalytic performance for methane oxidation as a function of reaction temperature for 5 wt% Pd 5 wt% CeO_2/Al_2O_3 (5P5C-A) catalyst where alumina was prepared via the SCS method and Pd and CeO_2 were introduced via impregnation and 5 wt% Pd 5 wt% CeO_2/Al_2O_3 SCS (5P5C-SCS) catalyst. Light-off measurements were carried out with 30 mg of catalyst at a total gas pressure of 1 atm with CH_4 (5% CH_4/Ar) to O_2 (5% O_2/Ar) v/v ratio of 2. Catalyst was activated by treating them with 30 mL min^{-1} of 5% O_2/Ar at 550 °C at a heating rate of 10 °C min^{-1}.

3. Materials and Methods

3.1. Catalyst Synthesis

A set of three Pd-based catalysts with different palladium and fixed ceria loadings (w/w%) namely 1% Pd/5% CeO_2/Al_2O_3, 2.5% Pd/5% CeO_2/Al_2O_3 and 5% Pd/5% CeO_2/Al_2O_3, were prepared and denoted as 1P5C-SCS, 2.5P5C-SCS and 5P5C-SCS, respectively. In a typical example to prepare 0.5 g of the 2.5% Pd/5% CeO_2/Al_2O_3 catalyst by the solution combustion synthesis technique, 0.0313 g of palladium(II) nitrate trihydrate ($Pd(NO_3)_2{\cdot}3H_2O$, BDH), 0.063 g of cereous(III) nitrate hexahydrate ($Ce(NO_3)_3{\cdot}6H_2O$, Fluka-Garantie, >99.0%) and 3.37 g of aluminum nitrate nonahydrate ($Al(NO_3)_3{\cdot}9H_2O$, Sigma Aldrich, Saint Louis, MO, USA, 99.9%) precursor salts were dissolved in 50 mL deionized water and stirred to give a homogeneous mixture. This was followed by the addition of 1.612 g of glycine (Sigma Aldrich, 98.5%) into the mixture to obtain oxidizer to fuel ratio of around 1/1.4. The resulting solution was then heated over a hot plate for combustion. The reaction is exothermic in nature and proceeds auto-thermally without further external heating after initiation of combustion. A detailed description of the synthesis procedure is provided elsewhere [31–33,35,44,47,53,67–71]. The synthesized nano-powder was then sintered in air by heating at a rate of 1 °C min^{-1} until it reached 800 °C where it was maintained for 3 h before cooling to room temperature at a rate of 1 °C min^{-1}.

The activity of the present SCS catalyst was benchmarked with two traditional palladium/alumina and palladium/ceria/alumina catalysts. In the two cases, the palladium content was fixed at 5 wt%. These catalysts were denoted as 5P-I and 5P5C-I, respectively. The traditional catalysts were prepared via wet impregnation methods. For the 5P-I, the required weight of the precursor salt ($Pd(NO_3)_2{\cdot}3H_2O$, BDH) was dissolved in deionized water and introduced to the pre-calcined alumina (SASOL) support drop-wise. Similarly, the 5P5C-I was synthesized but with the addition of the required weight of the precursor salt ($Pd(NO_3)_2{\cdot}3H_2O$) and cereous(III) nitrate hexahydrate ($Ce(NO_3)_3{\cdot}6H_2O$, Fluka-Garantie, >99.0%) to the pre-calcined alumina. The resultant slurries were stirred for 6 h followed by drying at 120 °C and then calcination at 800 °C for 4 h with +1 °C and −1 °C heating and cooling rates, respectively.

3.2. Catalyst Characterization

Samples were characterized using various analytical tools, such as sequential temperature-programmed reduction (TPR), N_2-adsorption/desorption (BET) analysis, powder X-ray diffraction (XRD) analysis, and X-ray photoelectron spectroscopy (XPS).

Detailed surface morphology and particle size of the calcined catalysts were revealed using high angle annular dark field (HAADF) HRTEM-EDS analysis. Samples for HRTEM-EDS analysis were prepared by dispersing calcined catalyst powder into tetrahydofuran (THF) by sonication. A drop of sample was then placed onto a 200-mesh copper grid coated with a holey carbon film. The HRTEM images were taken using a JEOL 2010F high-resolution field emission microscope (JEOL, Tokyo, Japan) at an operating voltage of 200 kV. HAADF images were recorded with a 0.7 nm HR probe and a Gatan annular dark field detector having a collection angle of 54.9 mrad. EDX spectra were recorded by using a PGT PRISM Si(Li) (Princeton Gamma-Tech Instruments, Princeton, NJ, USA).

The N_2 adsorption–desorption analysis was carried out using an automated gas adsorption analyzer (ASAP2024, Micrometrics, Norcross, GA, USA). Typically, 0.1 g of the sample was loaded in the pre-weighed quartz sample tube and degassed in the degasser port overnight at 120 °C under a flow of nitrogen to remove moisture and other impurities. After pre-treatment of samples, the specific surface area was determined by the BET method using nitrogen gas as adsorbate. The pore size distribution was determined from the desorption branch of the adsorption isotherm by the Barrett-Joyner-Halenda (BJH) method.

The X-ray diffraction (XRD) method was used to characterize the phase and structure of the catalysts. Room temperature XRD measurements were performed on a desktop X-ray diffractometer (Rigaku, MiniFlexII, Leatherhead, UK) equipped with a CuKα radiation source, at 30 kV and 15 mA, at a scanning angle (2θ) range of 5–80° at scanning speed of 4°/min. Specimens were prepared by packing around 0.3 g of sample powder into a glass holder.

Full elemental surface analysis was carried out using a photoelectron spectrometer (AXIS Ultra DLD, KRATOS, Manchestor, UK) equipped with an angular resolved XPS, a small spot XPS facilities and a Gas Cluster Ion Source (GCIS) for sample sputtering using monatomic Ar^+. Around 10 mg of the sample was placed in a gold-coated bronze stub and placed in the sample analysis chamber. Prior to XPS analysis, the surface of the samples was cleaned of adventitious carbon with an argon ion gun at an accelerating voltage of 4 KeV. The pressure in the analytical chamber during spectral acquisition was below 1.0×10^{-8} torr with the surface analysis depth ranging from ~30 to ~50 Å. The pass energy for the survey and high-resolution scans was 160 and 20 eV, respectively, while the accelerating voltage of monochromatized AlKα source was 15 kV.

Sequential temperature programmed reduction and temperature programmed oxidation (H_2-TPR/TPO) offer a useful tool to reveal the reduction behavior of different oxidized phases and metal to support interactions of the catalysts. Sequential H_2-TPR/TPO analyses of the calcined samples were carried out using ChemiSorb2750 (Micromeritics, Norcross, GA, USA) equipped with a thermal conductivity detector (TCD). This process consisted of two steps namely pretreatment and analysis. For pretreatment, 30 mg of the calcined sample was placed between two layers of quartz wool in a U-shaped quartz tube. The reactor temperature was raised to 200 °C at a rate of 10 °C min^{-1} in 20 mL min^{-1} of argon (Ar). The sample was degassed at this temperature for one hour and cooled down to 40 °C in an Ar flow. This step was then followed by H_2-TPR, performed by switching the flow to 25 cm^3 min^{-1} of 5 vol% H_2/Ar and heating from 40 °C to 900 °C at a rate of 10 °C min^{-1}. The tail gas directly passed to the thermal conductivity detector (TCD) to determine the hydrogen consumption. For TPO analysis, the reduced sample (after H_2-TPR step) was cooled down to 40 °C in a H_2/Ar flow followed by flushing with Ar for 15 min. The flow was then switched to 25 mL min^{-1} of 1 vol% O_2/Ar and the furnace temperature ramped from 40 °C to 900 °C at 10 °C min^{-1}.

3.3. Catalytic Activity Measurements

The methane oxidation catalytic performance investigated in a U-shaped quartz reactor connected with an online Quadrapole mass spectrometer HPR20 (Hidden Analytical, Warrington, UK). Light-off measurements were carried out with 30 mg of catalyst at a total gas pressure of 1 atm with CH_4 (5% CH_4/Ar) to O_2 (5% O_2/Ar) v/v ratio of 2. Experiments under wet conditions were conducted by admitting 18% steam into the reaction mixture via an HPLC pump. Prior to each experiment,

the catalyst was activated by treating with 5% O_2/Ar at 30 mL min^{-1} for 30 min at 500 °C. This step was followed by flushing the catalyst bed with 20 mL min^{-1} Ar for 20 min, raising the furnace temperature to 800 °C to record the light-off curves. Light-off curves were taken at heating and cooling rates of +10 and −10 K min^{-1}, respectively.

The CH_4 percent conversion is calculated using Equation (1);

$$CH_4 \text{ conversion } (\%) = \left[\frac{CH_4(\text{in}) - CH_4(\text{out})}{CH_4(\text{in})}\right] \times 100 \quad (1)$$

3.4. Effect of Reductive Pretreatment on Catalytic Activity

The effect of reductive pretreatment on the catalytic activity was also studied. The catalyst was reduced in flowing 30 mL min^{-1} pure H_2 at 300 °C for 30 min. The reaction temperature was then raised to 500 °C at a heating rate of 5 °C min^{-1} in flowing H_2. This step was followed by flushing the catalyst bed with 20 mL min^{-1} Ar for 20 min and then the inert gas was replaced by the required CH_4/O_2 gases mixture at a total gas pressure of 1 atm with O_2 (5% O_2/Ar) to CH_4 (5% CH_4/Ar) v/v ratio of 2. The cooling cycle in the temperature range between 500 °C and 200 °C was then taken at cooling rates of −5 K min^{-1}.

3.5. Effects of the Type of Alumina Support on Catalytic Activity

In order to eliminate any difference in the catalytic activity caused by the type of the alumina as support, one more catalyst with a composition of 5 wt% Pd 5 wt% CeO_2/Al_2O_3 was also synthesized. This catalyst was denoted as 5P5C-A. In this case, as a first step, the alumina support was prepared by the SCS method according to the procedure mentioned in Section 3.1. The synthesized powder was calcined at 800 °C for 3 h with +1 °C and −1 °C heating and cooling rates, respectively. This was followed by the addition of the required weight of the precursor salts of ($Pd(NO_3)_2 \cdot 3H_2O$, BDH) and cereous(III) nitrate hexahydrate ($Ce(NO_3)_3 \cdot 6H_2O$, Fluka-Garantie, >99.0%) dissolved in deionized water. The resultant slurry was stirred for 6 h followed by drying at 120 °C and then calcination at 800 °C for 4 h with +1 °C and −1 °C heating and cooling rates, respectively. The comparison between catalytic activity during methane oxidation over 5P5C-SCS and 5P5C-A was performed to investigate any difference between the two catalysts caused by the type of alumina used as support.

4. Conclusions

Active and stable alumina supported Pd/CeO_2 catalysts were prepared via one-step SCS. The catalyst active phase, believed to be a solid solution of Pd inserted into CeO_2, segregated within the surface region of the alumina support. The catalyst worked out with 100% efficiency for methane oxidation at temperatures above 400 °C. The high activity is suggested to be due to the "intrinsic" insertion of Ce^{3+} ions and oxygen vacancies, both associated with the insertion of highly ionized $Pd^{+(2+x)}$ ions into the ceria lattice. At 550 °C, compared to the traditional catalyst, the rates of methane decomposition under similar reaction over the SCS catalyst were higher by more than a factor of 18.

Acknowledgments: This paper was made possible by an NPRP Grant #6-290-1-059 from the Qatar National Research Fund (a member of Qatar Foundation). The statements made herein are solely the responsibility of the authors.

Author Contributions: Mahmoud M. Khader provided the concept of this research as well as managed all of the writing and experimental processes as corresponding author; Mohammed J. Al-Marri designed the experiments for catalytic evaluation; Sardar Ali analyzed the data and carried out the XPS experiments; Ahmed G. Abdelmoneim performed the experiments for catalytic evaluation.

Conflicts of Interest: The authors declare no conflicts of interest.

References

1. Rivero-Mendoza, D.E.; Stanley, J.N.; Scott, J.; Aguey-Zinsou, K.-F. An alumina-supported Ni-La-based catalyst for producing synthetic natural gas. *Catalysts* **2016**, *6*, 170. [CrossRef]
2. Gélin, P.; Primet, M. Complete oxidation of methane at low temperature over noble metal based catalysts: A review. *Appl. Catal. B* **2002**, *39*, 1–37. [CrossRef]
3. Samimi, F.; Rahimpour, M.R.; Shariati, A. Development of an Efficient Methanol Production Process for Direct CO_2 Hydrogenation over a $Cu/ZnO/Al_2O_3$ Catalyst. *Catalysts* **2017**, *7*, 332. [CrossRef]
4. Persson, K.; Jansson, K.; Järås, S.G. Characterisation and microstructure of Pd and bimetallic Pd–Pt catalysts during methane oxidation. *J. Catal.* **2007**, *245*, 401–414. [CrossRef]
5. Ciuparu, D.; Lyubovsky, M.R.; Altman, E.; Pfefferle, L.D.; Datye, A. Catalytic combustion of methane over palladium-based catalysts. *Catal. Rev.* **2002**, *44*, 593–649. [CrossRef]
6. Gélin, P.; Urfels, L.; Primet, M.; Tena, E. Complete oxidation of methane at low temperature over Pt and Pd catalysts for the abatement of lean-burn natural gas fuelled vehicles emissions: Influence of water and sulphur containing compounds. *Catal. Today* **2003**, *83*, 45–57. [CrossRef]
7. Gholami, R.; Alyani, M.; Smith, K.J. Deactivation of Pd catalysts by water during low temperature methane oxidation relevant to natural gas vehicle converters. *Catalysts* **2015**, *5*, 561–594. [CrossRef]
8. Lapisardi, G.; Urfels, L.; Gélin, P.; Primet, M.; Kaddouri, A.; Garbowski, E.; Toppi, S.; Tena, E. Superior catalytic behaviour of Pt-doped Pd catalysts in the complete oxidation of methane at low temperature. *Catal. Today* **2006**, *117*, 564–568. [CrossRef]
9. Persson, K.; Ersson, A.; Jansson, K.; Iverlund, N.; Järås, S. Influence of co-metals on bimetallic palladium catalysts for methane combustion. *J. Catal.* **2005**, *231*, 139–150. [CrossRef]
10. Schwartz, W.R.; Pfefferle, L.D. Combustion of Methane over Palladium-Based Catalysts: Support Interactions. *J. Phys. Chem. C* **2012**, *116*, 8571–8578. [CrossRef]
11. Chin, Y.-H.; Buda, C.; Neurock, M.; Iglesia, E. Consequences of Metal–Oxide Interconversion for C–H Bond Activation during CH_4 Reactions on Pd Catalysts. *J. Am. Chem. Soc.* **2013**, *135*, 15425–15442. [CrossRef] [PubMed]
12. Venezia, A.M.; Di Carlo, G.; Pantaleo, G.; Liotta, L.F.; Melaet, G.; Kruse, N. Oxidation of CH_4 over Pd supported on TiO_2-doped SiO_2: Effect of Ti(IV) loading and influence of SO_2. *Appl. Catal. B* **2009**, *88*, 430–437. [CrossRef]
13. Meng, L.; Lin, J.-J.; Pu, Z.-Y.; Luo, L.-F.; Jia, A.-P.; Huang, W.-X.; Luo, M.-F.; Lu, J.-Q. Identification of active sites for CO and CH_4 oxidation over $PdO/Ce_{1-x}PdxO_{2-\delta}$ catalysts. *Appl. Catal. B* **2012**, *119–120*, 117–122. [CrossRef]
14. Zhu, G.; Han, J.; Zemlyanov, D.Y.; Ribeiro, F.H. Temperature Dependence of the Kinetics for the Complete Oxidation of Methane on Palladium and Palladium Oxide. *J. Phys. Chem. B* **2005**, *109*, 2331–2337. [CrossRef] [PubMed]
15. Domingos, D.; Rodrigues, L.M.T.S.; Frety, R.; Brandao, S.T. Combustion of Methane Using Palladium Catalysts Supported in Alumina or Zirconia. *Combust. Sci. Technol.* **2014**, *186*, 518–528. [CrossRef]
16. Grunwaldt, J.-D.; Vegten, N.V.; Baiker, A. Insight into the structure of supported palladium catalysts during the total oxidation of methane. *Chem. Commun.* **2007**, 4635–4637. [CrossRef] [PubMed]
17. Sanchez, M.G.; Gazquez, J.L. Oxygen vacancy model in strong metal-support interaction. *J. Catal.* **1987**, *104*, 120–135. [CrossRef]
18. Van Vegten, N.; Maciejewski, M.; Krumeich, F.; Baiker, A. Structural properties, redox behaviour and methane combustion activity of differently supported flame-made Pd catalysts. *Appl. Catal. B* **2009**, *93*, 38–49. [CrossRef]
19. Matam, S.K.; Aguirre, M.; Weidenkaff, A.; Ferri, D. Revisiting the problem of active sites for methane combustion on Pd/Al_2O_3 by operando XANES in a lab-scale fixed-bed reactor. *J. Phys. Chem. C* **2010**, *114*, 9439–9443. [CrossRef]
20. Farrauto, R.J.; Hobson, M.C.; Kennelly, T.; Waterman, E.M. Catalytic chemistry of supported palladium for combustion of methane. *Appl. Catal. A* **1992**, *81*, 227–237. [CrossRef]
21. Xiao, L.-H.; Sun, K.-P.; Xu, X.-L.; Li, X.-N. Low-temperature catalytic combustion of methane over Pd/CeO_2 prepared by deposition–precipitation method. *Catal. Commun.* **2005**, *6*, 796–801. [CrossRef]

22. Colussi, S.; Trovarelli, A.; Groppi, G.; Llorca, J. The effect of CeO_2 on the dynamics of Pd–PdO transformation over Pd/Al_2O_3 combustion catalysts. *Catal. Commun.* **2007**, *8*, 1263–1266. [CrossRef]
23. Colussi, S.; Gayen, A.; Farnesi Camellone, M.; Boaro, M.; Llorca, J.; Fabris, S.; Trovarelli, A. Nanofaceted Pd–O Sites in Pd–Ce Surface Superstructures: Enhanced Activity in Catalytic Combustion of Methane. *Angew. Chem. Int. Ed.* **2009**, *48*, 8481–8484. [CrossRef] [PubMed]
24. Mayernick, A.D.; Janik, M.J. Methane oxidation on Pd–Ceria: A DFT study of the mechanism over $Pd_xCe_{1-x}O_2$, Pd, and PdO. *J. Catal.* **2011**, *278*, 16–25. [CrossRef]
25. Cargnello, M.; Jaén, J.J.D.; Garrido, J.C.H.; Bakhmutsky, K.; Montini, T.; Gámez, J.J.C.; Gorte, R.J.; Fornasiero, P. Exceptional Activity for Methane Combustion over Modular $Pd@CeO_2$ Subunits on Functionalized Al_2O_3. *Science* **2012**, *337*, 713–717. [CrossRef] [PubMed]
26. Bakhmutsky, K.; Wieder, N.L.; Cargnello, M.; Galloway, B.; Fornasiero, P.; Gorte, R.J. A versatile route to core-shell catalysts: Synthesis of dispersible M@oxide (M = Pd, Pt; Oxide = TiO_2, ZrO_2) nanostructures by self-assembly. *ChemSusChem* **2012**, *5*, 140–148. [CrossRef] [PubMed]
27. Monai, M.; Montini, T.; Melchionna, M.; Duchoň, T.; Kúš, P.; Chen, C.; Tsud, N.; Nasi, L.; Prince, K.C.; Veltruská, K.; et al. The effect of sulfur dioxide on the activity of hierarchical Pd-based catalysts in methane combustion. *Appl. Catal. B* **2017**, *202*, 72–83. [CrossRef]
28. Chen, C.; Yeh, Y.-H.; Cargnello, M.; Murray, C.B.; Fornasiero, P.; Gorte, R.J. Methane Oxidation on $Pd@ZrO_2/Si–Al_2O_3$ Is Enhanced by Surface Reduction of ZrO_2. *ACS Catal.* **2014**, *4*, 3902–3909. [CrossRef]
29. Schwartz, W.R.; Ciuparu, D.; Pfefferle, L.D. Combustion of Methane over Palladium-Based Catalysts: Catalytic Deactivation and Role of the Support. *J. Phys. Chem. C* **2012**, *116*, 8587–8593. [CrossRef]
30. Onn, T.M.; Arroyo-Ramirez, L.; Monai, M.; Oh, T.-S.; Talati, M.; Fornasiero, P.; Gorte, R.J.; Khader, M.M. Modification of Pd/CeO_2 catalyst by Atomic Layer Deposition of ZrO_2. *Appl. Catal. B* **2016**, *197*, 280–285. [CrossRef]
31. Aruna, S.T.; Mukasyan, A.S. Combustion synthesis and nanomaterials. *Curr. Opin. Solid State Mater. Sci.* **2008**, *12*, 44–50. [CrossRef]
32. González-Cortés, S.L.; Imbert, F.E. Fundamentals, properties and applications of solid catalysts prepared by solution combustion synthesis (SCS). *Appl. Catal. A* **2013**, *452*, 117–131. [CrossRef]
33. Suresh, K.; Patil, K.C.; Rao, K.J. *Perspectives in Solid State Chemistry*; Narosa Publishing House: New Delhi, India, 1995.
34. Monai, M.; Montini, T.; Chen, C.; Fonda, E.; Gorte, R.J.; Fornasiero, P. Methane Catalytic Combustion over Hierarchical $Pd@CeO_2/Si-Al_2O_3$: Effect of the Presence of Water. *ChemCatChem* **2015**, *7*, 2038–2046. [CrossRef]
35. Specchia, S.; Finocchio, E.; Busca, G.; Palmisano, P.; Specchia, V. Surface chemistry and reactivity of ceria–zirconia-supported palladium oxide catalysts for natural gas combustion. *J. Catal.* **2009**, *263*, 134–145. [CrossRef]
36. Priolkar, K.R.; Bera, P.; Sarode, P.R.; Hegde, M.S.; Emura, S.; Kumashiro, R.; Lalla, N.P. Formation of $Ce_{1-x}Pd_xO_{2-\delta}$ Solid Solution in Combustion-Synthesized Pd/CeO_2 Catalyst: XRD, XPS, and EXAFS Investigation. *Chem. Mater.* **2002**, *14*, 2120–2128. [CrossRef]
37. Bera, P.; Patil, K.C.; Jayaram, V.; Subbanna, G.N.; Hegde, M.S. Ionic Dispersion of Pt and Pd on CeO_2 by Combustion Method: Effect of Metal–Ceria Interaction on Catalytic Activities for NO Reduction and CO and Hydrocarbon Oxidation. *J. Catal.* **2000**, *196*, 293–301. [CrossRef]
38. Colussi, S.; Gayen, A.; Boaro, M.; Llorca, J.; Trovarelli, A. Influence of Different Palladium Precursors on the Properties of Solution-Combustion-Synthesized Palladium/Ceria Catalysts for Methane Combustion. *ChemCatChem* **2015**, *7*, 2222–2229. [CrossRef]
39. Gil, S.; Garcia-Vargas, M.J.; Liotta, F.L.; Pantaleo, G.; Ousmane, M.; Retailleau, L.; Giroir-Fendler, A. Catalytic Oxidation of Propene over Pd Catalysts Supported on CeO_2, TiO_2, Al_2O_3 and M/Al_2O_3 Oxides (M = Ce, Ti, Fe, Mn). *Catalysts* **2015**, *5*, 671–689. [CrossRef]
40. Hong, J.W.; Lee, Y.W.; Kim, M.; Kang, S.W.; Han, S.W. One-pot synthesis and electrocatalytic activity of octapodal Au–Pd nanoparticles. *Chem. Commun.* **2011**, *47*, 2553–2555. [CrossRef] [PubMed]
41. Wu, C. Solvothermal synthesis of N-doped CeO_2 microspheres with visible light-driven photocatalytic activity. *Mater. Lett.* **2015**, *139*, 382–384. [CrossRef]

42. Chiu, P.-C.; Ku, Y.; Wu, Y.-L.; Wu, H.-C.; Kuo, Y.-L.; Tseng, Y.-H. Characterization and evaluation of prepared Fe_2O_3/Al_2O_3 oxygen carriers for chemical looping process. *Aerosol Air Qual. Res.* **2014**, *14*, 981–990. [CrossRef]
43. Seo, C.; Yi, E.; Nahata, M.; Laine, R.M.; Schwank, J.W. Facile, one-pot synthesis of Pd@CeO_2 core@shell nanoparticles in aqueous environment by controlled hydrolysis of metalloorganic cerium precursor. *Mater. Lett.* **2017**, *206*, 105–108. [CrossRef]
44. Mistri, R.; Rahaman, M.; Llorca, J.; Priolkar, K.R.; Colussi, S.; Ray, B.C.; Gayen, A. Liquid phase selective oxidation of benzene over nanostructured $Cu_xCe_{1-x}O_{2-\delta}$ ($0.03 \leq x \leq 0.15$). *J. Mol. Catal. A Chem.* **2014**, *390*, 187–197. [CrossRef]
45. Th, P.; Zimmermann, R.; Steiner, P.; Hüfner, S. The electronic structure of PdO found by photoemission (UPS and XPS) and inverse photoemission (BIS). *J. Phys. Condens. Matter.* **1997**, *9*, 3987–3999. [CrossRef]
46. Brun, M.; Berthet, A.; Bertolini, J.C. XPS, AES and Auger parameter of Pd and PdO. *J. Electron. Spectrosc. Relat. Phenom.* **1999**, *104*, 55–60. [CrossRef]
47. Shinde, V.M.; Madras, G. Kinetic studies of ionic substituted copper catalysts for catalytic hydrogen combustion. *Catal. Today* **2012**, *198*, 270–279. [CrossRef]
48. Huang, H.; Ye, X.; Huang, H.; Zhang, L.; Leung, D.Y.C. Mechanistic study on formaldehyde removal over Pd/TiO_2 catalysts: Oxygen transfer and role of water vapor. *Chem. Eng. J.* **2013**, *230*, 73–79. [CrossRef]
49. Ihm, S.-K.; Jun, Y.-D.; Kim, D.-C.; Jeong, K.-E. Low-temperature deactivation and oxidation state of Pd/γ-Al_2O_3 catalysts for total oxidation of n-hexane. *Catal. Today* **2004**, *93–95*, 149–154. [CrossRef]
50. Aznárez, A.; Korili, S.A.; Gil, A. The promoting effect of cerium on the characteristics and catalytic performance of palladium supported on alumina pillared clays for the combustion of propene. *Appl. Catal. A* **2014**, *474*, 95–99. [CrossRef]
51. Bi, Y.; Lu, G. Catalytic CO oxidation over palladium supported NaZSM-5 catalysts. *Appl. Catal. B* **2003**, *41*, 279–286. [CrossRef]
52. Venezia, A.M.; Di Carlo, G.; Liotta, L.F.; Pantaleo, G.; Kantcheva, M. Effect of Ti(IV) loading on CH_4 oxidation activity and SO_2 tolerance of Pd catalysts supported on silica SBA-15 and HMS. *Appl. Catal. B* **2011**, *106*, 529–539. [CrossRef]
53. Vita, A.; Cristiano, G.; Italiano, C.; Pino, L.; Specchia, S. Syngas production by methane oxy-steam reforming on Me/CeO_2 (Me = Rh, Pt, Ni) catalyst lined on cordierite monoliths. *Appl. Catal. B* **2015**, *162*, 551–563. [CrossRef]
54. Scanlon, D.O.; Morgan, B.J.; Watson, G.W. The origin of the enhanced oxygen storage capacity of $Ce_{1-x}(Pd/Pt)_xO_2$. *Phys. Chem. Chem. Phys.* **2011**, *13*, 4279–4284. [CrossRef] [PubMed]
55. Zhang, J.; Yang, H.; Wang, S.; Liu, W.; Liu, X.; Guo, J.; Yang, Y. Mesoporous CeO_2 nanoparticles assembled by hollow nanostructures: Formation mechanism and enhanced catalytic properties. *CrystEngComm* **2014**, *16*, 8777–8785. [CrossRef]
56. Harrison, B.; Diwell, A.F.; Hallett, C. Promoting Platinum Metals by Ceria. *Platin. Met. Rev.* **1988**, *32*, 73–83.
57. Huang, M.; Fabris, S. Role of surface peroxo and superoxo species in the low-temperature oxygen buffering of ceria: Density functional theory calculations. *Phys. Rev. B* **2007**, *75*, 081404. [CrossRef]
58. Fouladvand, S.; Schernich, S.; Libuda, J.; Grönbeck, H.; Pingel, T.; Olsson, E.; Skoglundh, M.; Carlsson, P.-A. Methane oxidation over Pd supported on ceria–alumina under rich/lean cycling conditions. *Top. Catal.* **2013**, *56*, 410–415. [CrossRef]
59. Su, Y.-Q.; Filot, I.A.; Liu, J.-X.; Hensen, E.J. Stable Pd-doped Ceria Structures for CH_4 Activation and CO Oxidation. *ACS Catal.* **2017**. [CrossRef] [PubMed]
60. Su, Y.-Q.; Liu, J.-X.; Filot, I.A.; Hensen, E.J. Theoretical study of ripening mechanisms of Pd clusters on Ceria. *Chem. Mater.* **2017**, *29*, 9456–9462. [CrossRef] [PubMed]
61. Primavera, A.; Trovarelli, A.; de Leitenburg, C.; Dolcetti, G.; Llorca, J. Reactivity and characterization of Pd-containing ceria-zirconia catalysts for methane combustion. *Stud. Surf. Sci. Catal.* **1998**, 87–92. [CrossRef]
62. De Rogatis, L.; Cargnello, M.; Gombac, V.; Lorenzut, B.; Montini, T.; Fornasiero, P. Embedded phases: A way to active and stable catalysts. *ChemSusChem* **2010**, *3*, 24–42. [CrossRef] [PubMed]
63. Yeung, C.M.; Yu, K.M.K.; Fu, Q.J.; Thompsett, D.; Petch, M.I.; Tsang, S.C. Engineering Pt in ceria for a maximum metal—Support interaction in catalysis. *J. Am. Chem. Soc.* **2005**, *127*, 18010–18011. [CrossRef] [PubMed]

64. Tedsree, K.; Li, T.; Jones, S.; Chan, C.W.A.; Yu, K.M.K.; Bagot, P.A.; Marquis, E.A.; Smith, G.D.; Tsang, S.C.E. Hydrogen production from formic acid decomposition at room temperature using a Ag-Pd core-shell nanocatalyst. *Nat. Nanotechnol.* **2011**, *6*, 302–307. [CrossRef] [PubMed]
65. Colussi, S.; Gayen, A.; Llorca, J.; de Leitenburg, C.; Dolcetti, G.; Trovarelli, A. Catalytic performance of solution combustion synthesized alumina-and ceria-supported Pt and Pd nanoparticles for the combustion of propane and dimethyl ether (DME). *Ind. Eng. Chem. Res.* **2012**, *51*, 7510–7517. [CrossRef]
66. Burch, R.; Urbano, F.J. Investigation of the active state of supported palladium catalysts in the combustion of methane. *Appl. Catal. A* **1995**, *124*, 121–138. [CrossRef]
67. Kumar, A.; Ashok, A.; Bhosale, R.R.; Saleh, M.A.H.; Almomani, F.A.; Al-Marri, M.; Khader, M.M.; Tarlochan, F. In situ DRIFTS Studies on Cu, Ni and CuNi catalysts for Ethanol Decomposition Reaction. *Cataly. Lett.* **2016**, *146*, 778–787. [CrossRef]
68. Piumetti, M.; Fino, D.; Russo, N. Mesoporous manganese oxides prepared by solution combustion synthesis as catalysts for the total oxidation of VOCs. *Appl. Catal., B* **2015**, *163*, 277–287. [CrossRef]
69. Kumar, A.; Mukasyan, A.S.; Wolf, E.E. Combustion synthesis of Ni, Fe and Cu multi-component catalysts for hydrogen production from ethanol reforming. *Appl. Catal. A* **2011**, *401*, 20–28. [CrossRef]
70. Ali, S.; Al-Marri, M.J.; Abdelmoneim, A.G.; Kumar, A.; Khader, M.M. Catalytic evaluation of nickel nanoparticles in methane steam reforming. *Int. J. Hydrogen Energy* **2016**, *41*, 22876–22885. [CrossRef]
71. Ashok, A.; Kumar, A.; Bhosale, R.R.; Saleh, M.A.H.; Ghosh, U.K.; Al-Marri, M.; Almomani, F.A.; Khader, M.M.; Tarlochan, F. Cobalt oxide nanopowder synthesis using cellulose assisted combustion technique. *Ceram. Int.* **2016**, *42*, 12771–12777. [CrossRef]